Mg-Based Metallic Glass-Polymer Composites: Investigation of Structure, Thermal Properties, and Biocompatibility

Adit Sharma [1], **Alexey Kopylov [2]**, **Mikhail Zadorozhnyy [1]**, **Andrei Stepashkin [1]**, **Vera Kudelkina [2]**, **Jun-Qiang Wang [3]**, **Sergey Ketov [4]**, **Margarita Churyukanova [1]**, **Dmitri Louzguine-Luzgin [5,6]**, **Baran Sarac [4]**, **Jürgen Eckert [4,7]**, **Sergey Kaloshkin [1]**, **Vladislav Zadorozhnyy [1,4,*]** and **Hidemi Kato [8]**

[1] National University of Science and Technology «MISiS», Leninsky Prosp., 4, 119049 Moscow, Russia; adit15@yandex.com (A.S.); zadorozhnyy.mihail@gmail.com (M.Z.); a.stepashkin@yandex.ru (A.S.); mch@misis.ru (M.C.); kaloshkin@misis.ru (S.K.)

[2] Institute of Human Morphology, Tsiurupy str., 3, 117418 Moscow, Russia; dreadnought88@gmail.com (A.K.); verakudelkina8047@gmail.com (V.K.)

[3] CAS Key Laboratory of Magnetic Materials and Devices, and Zhejiang Province Key Laboratory of Magnetic Materials and Application Technology, Ningbo Institute of Materials Technology and Engineering, Chinese Academy of Sciences, Ningbo 315201, China; jqwang@nimte.ac.cn

[4] Erich Schmid Institute of Materials Science, Austrian Academy of Sciences, Jahnstraße 12, 8700 Leoben, Austria; ketov.sergey@gmail.com (S.K.); baran.sarac@oeaw.ac.at (B.S.); juergen.eckert@unileoben.ac.at (J.E.)

[5] WPI Advanced Institute for Materials Research, Tohoku University, Sendai 980-8577, Japan; dml@wpi-aimr.tohoku.ac.jp

[6] MathAM-OIL, National Institute of Advanced Industrial Science and Technology (AIST), Sendai 980-8577, Japan

[7] Department of Materials Science, Chair of Materials Physics, Montanuniversität Leoben, Jahnstraße 12, 8700 Leoben, Austria

[8] Institute for Materials Research (IMR), Tohoku University, Sendai 980-8577, Japan; hikato@imr.tohoku.ac.jp

* Correspondence: vuz@misis.ru; Tel.: +7-(495)738-44-13

check for updates

Abstract: In this work, the biomedical applicability and physical properties of magnesium-based metallic glass/polycaprolactone (PCL) composites are explored. The composites were fabricated via mechanical alloying and subsequent coextrusion. The coextrusion process was carried out at a temperature near to the supercooled liquid region of the metallic glass and the viscous region of the polymer. The structures, as well as thermal and mechanical properties of the obtained samples were characterized, and in vivo investigations were undertaken. The composite samples possess acceptable thermal and mechanical properties. Tensile tests indicate the ability of the composites to withstand more than 100% deformation. In vivo studies reveal that the composites are biologically compatible and could be promising for biomedical applications.

1. Introduction

Human bones have a natural ability to heal and repair defects, for example, fractures. However, this natural healing capacity is insufficient to repair large fractures; hence, defect and tissue engineering are required to restore bones to their natural state [1,2]. Grafting is one of the possible ways to boost the repair capability of bones. Autologous bone has a similar mineral

composition and cell structure to native human bones. However, there are serious limitations involving the graft size and damage to the donor zone [3]. Allografts that are taken from other persons or animals (in this case it is called a xenograft) address size limitations but are known to have limited osteoinduction, limited availability, a high cost associated with storing allografts in biobanks [4], and the danger of infection [5]. These disadvantages can be overcome by synthetic materials, colonized cells, and tissue-engineered construction [6]. They can be inert or bioactive and degradable or nondegradable in nature [6]. Inert materials do not react with the organism, while bioactive materials interact with tissues. Preferably, the material should have a Young's modulus similar to that of bone to avoid stress shielding [1]. Another very important property of the material is its biocompatibility: the material should not cause acute inflammation, necrosis, or edema [1]. Furthermore, the material should induce osteogenesis after implantation [1,7].

Biodegradable materials can be an effective substitute for bioinert compounds, as there is no need for implant removal, and hence they are an effective solution for permanent implants. Mg-based alloys can degrade over time, which avoids the need for additional surgery and also prevents internal injuries during the removal of implants. Magnesium, calcium, zinc, and iron are generally employed for biodegradable metallic implants, and the human body can tolerate a small number of elements, including Mn, Ca, and Zn [8]. Ca is a major component of bone and can improve bone growth [9]. Zn is used as an alloy strengthening material [10]. In the case of Zn and Fe, their degradation products cause adverse effects at the implant site [11,12]. Moreover, magnesium plays a key role in the mammalian body and is considered as an essential element for many enzymes [13]. Magnesium is generally used as an alloy [14–16], and the density of magnesium-based alloys (1.74–2.0 g/cm^3) is similar to that of bone (1.8–2.1 g/cm^3). The strength of Mg alloys can be enhanced via dispersion strengthening and solid solution strengthening [17]. Magnesium-based metallic glasses are safe and nontoxic in nature; however, they are brittle, and the implants cause the formation of hydrogen bubbles produced by the corrosive reaction $Mg + 2H_2O \rightarrow Mg^{2+} + 2OH^- + H_2$ [18]. The high strength, low elastic modulus, and large elasticity of magnesium alloys can assist in enhancing human metabolism (for DNA and RNA functioning) [19,20]. The major drawbacks associated with magnesium-based alloys are their brittle nature and that their degradation and corrosion rates are higher than the rate of bone formation [21]. These issues can cause the implant to lose structural integrity before complete healing. Another drawback of biocompatibility is the aforementioned formation of hydrogen bubbles. While it does not seem to be a problem in cardiovascular stents, in bone implants gas pockets are a problem because of the poor transport mechanisms. This might require to remove gas pockets with punctures. While imposing some mechanical stress by pressure may stimulate bone formation, gas bubbles may prevent cell migration and vascularization. [22]. Although, Zimmermann et al. [23] showed that gas pockets disappear after several weeks. The factors that influence the degradation of magnesium include blood plasma, temperature, and protein [24]. Metallic glasses (MGs) [25,26] exhibit a relatively low elastic modulus that is closer to that of bone compared with their crystalline counterparts [27]. Some MGs, such as Sr-, Ca-, and Mg-based systems, exhibit an elastic modulus that is comparable to the human cortical bone and is favored for the use as an implant material because it can decrease atrophy of the cortical bone [28]. Mg-Zn-Ca bulk metallic glasses generally exhibit improved corrosion resistance, good biocompatibility, higher strength, and lower elastic modulus than pure Mg and commercial crystalline Mg-alloys [27]. The corrosion properties in simulated body fluid (SBF) and the in vitro cell compatibility of two $Mg_{66}Zn_{30}Ca_4$ and $Mg_{70}Zn_{25}Ca_5$ bulk metallic glasses (BMGs) were examined and compared with commercial Mg alloys in Reference [28]. It was confirmed that metallic glasses show better corrosion resistance than pure Mg and commercial Mg alloys. The two Mg-based BMGs had ~3-times higher compression strength having only three-fourths of the elastic modulus of pure Mg [27].

These advantages make Mg-Zn-Ca BMGs promising candidates for biodegradable implant materials. The incorporation of crystalline phases via annealing at high temperatures or by composition variation could increase the hardness and strength of the Mg-Zn-Ca alloys but could deteriorate the degradation behavior because of micro-galvanic corrosion. The poor ductility and limited glass-forming

ability are also two key factors impeding the application of Mg-Zn-Ca BMGs as biodegradable materials. However, the plasticity of Mg-Zn-Ca BMGs can be significantly improved by proper minor alloying with Yb [29]. This can be attributed to the increased nucleation of shear bands and enlarged plastic deformation zones. There remains significant scope for improving the biocorrosion resistance of Mg-based BMGs so that it is comparable to the recovery period of organisms and bones.

Ultra-high molecular weight polycaprolactone (PCL), polyethylene, and polyhydroxybutyrate are polymers that are frequently used as biomaterials [30]. PCL has good mechanical properties and biocompatibility and is used for bone and tracheal reconstruction [31]. It has been well studied, is widely available, and can be used for three-dimensional printing [32]. Furthermore, it accelerates cell growth within the implant, which makes it very useful for implant and tissue-engineered construction [33]. PCL shows the best results in combination with other materials. For example, PCL and starch derivatives composite show an increase in the modulus and thermal properties of the composites [34]. The addition of apatite crystals may create pores inside the material that allows the material to be filled with cells both inside and on the surface [35]. This occupation also improves bone regeneration after the placement of the implant into the defect. Minerals increase the osteoconductivity and osteoinductivity by stimulating osteogenic differentiation of bone-marrow-derived mesenchymal stem cells and thus enhance osteogenesis [36].

While there are many potential types of biomaterials, each has its own advantages and disadvantages with respect to their mechanical and biological properties. The best results are achieved by combinations of materials because this allows for the disadvantages of the respective materials to be overcome [34].

Metallic glasses with low glass transition temperatures near the softening temperature of the polymer can be used to produce metallic glass-polymer composites [37,38]. This feature allows for the cothermal-plastic deformation of the composite. A twist extrusion technique was used for processing polymers with a metallic glass to improve their mechanical properties [39].

Mg-based metallic glasses are promising biomaterials for medical applications when combined with biocompatible polymers. For example, a composite material based on high-density polyethylene (HDPE) reinforced with $Mg_{67.5}Ca_5Zn_{27.5}$ metallic glass (~10 wt.%) was obtained by coextrusion and compression [38]. The coextrusion and compression procedures were performed in between the glass transition temperature (T_g) and crystallization temperature (T_x) of the metallic glass, which improves the mechanical properties of the overall composite. The polymer was in the viscous form near the glass transition temperature of the metallic glass; hence, it was feasible to form a composite. It was found that the composite samples (HDPE/$Mg_{67.5}Ca_5Zn_{27.5}$) adhered well with each other and had good thermal conductivity [38]. The thermal properties of biomaterials are important for the analysis of the heat transfer, and the lifetime of implants under specific temperatures depend on the thermal conductivity. Therefore, biomaterials should have the ability to transfer thermal energy with respect to a temperature gradient [40].

In other reported studies, composite materials based on $Cu_{54}Pd_{28}P_{18}$ metallic glass and polytetrafluoroethylene (PTFE of ~1 mass%) [41] and $Al_{85}Y_8Ni_5Co_2$ metallic glass and polyethylene terephthalate polymer [42] were prepared via ball milling and subsequent spark plasma sintering (SPS). The mechanical properties of the composites were significantly enhanced and mechanical and structural characterization of the obtained metallic glass/polymer composite samples revealed that the composite could be used in non-load-bearing applications.

In the present work, a polycaprolactone (PCL) matrix was reinforced with $Mg_{66}Zn_{30}Ca_4$ metallic glass to produce composites for bioapplication. Mechanical alloying at room temperature and coextrusion of the composite powder blends in the supercooled liquid temperature region of the metallic glass and close to the softening temperature of the polymer were performed. The physical and mechanical properties of the obtained composites were investigated. Previous reports [29] investigated magnesium-based metallic glasses in vitro that were also alloyed with ytterbium (Yb) with an atomic concentration of 2 and 4 at.%. These in vitro studies confirmed the improved biocompatibility of

the magnesium-based metallic glass via apoptosis and cytoskeleton staining assays. In this work, composites based on a similar composition as the magnesium-based metallic glass reported earlier in ref. [29] were obtained and mixed with the biodegradable polymer (PCL).In vivo testing was performed to check the biocompatibility of the samples after implantation into the organism.

2. Materials and Methods

2.1. Alloy Preparation

An ingot of $Mg_{66}Zn_{30}Ca_4$ alloy was prepared via induction melting (Diavac Ltd., Yachiyo, Chiba, Japan) in an argon atmosphere from a mixture of pure Mg, Ca, and Zn (99% purity). Single copper roller melt spinning (under argon) was used for the preparation of 4.7–4.9 mm wide metallic glass (MG) ribbons. The thickness of the obtained ribbons was 20–30 μm. The average granular size of polycaprolactone (PCL) (Floroplast-4 mark) was ~3 mm.

2.2. Ball Milling

Fragmentation of the metallic glass ribbons was done in a high-energy water-cooled AGO-2S planetary ball mill (CJSC "NOVITS", Novosibirsk, Russian Federation) with a rotation speed of 840 min^{-1}, under argon. The used steel balls had a diameter of 4 mm, and the ball-to-powder mass ratio was 10:1. The milling of the metallic glass was repeated four times for 3 min each to avoid a potential temperature increase inside the vial [43]. The total duration of the ball milling of the metallic glass was 12 min.

2.3. Co-Extrusion Process

After ball milling, the composite PCL/MG powder was further mixed using a desktop high-speed twin-screw extruder (Thermo Scientific Haake MiniLab, Waltham, MA, USA) with a modular screw and a barrel. The working temperature in the extruder was between 120 and 130 °C; stirring was carried out for 10 min each. This temperature range (120–130 °C) was optimal for reaching low viscosity in both PCL melt and metallic glass while avoiding crystallization of the latter. After extrusion, the resulting metallic glass/polymer mixture was placed in an injection-molding machine (Thermo Scientific Haake Mini-Jet, Waltham, MA, USA). Using the injection-molding machine, the mixture was used to form the final samples in air.

Composite samples of different proportions were made by varying the ratio of polymer and metallic glass (in wt.%): 50:50, 75:25, and 90:10 (polymer to metallic glass ratio). Composites with metallic glass contents of more than 50 wt.% were difficult to produce in the extruder because there was a specific maximum concentration of the metal that the extruder could use.

2.4. X-ray Diffraction

The phase composition and structure of the materials after the different processing steps were determined via X-ray diffraction (XRD) on a DRON diffractometer (Research and production enterprise "Bourevestnik", Saint Petersburg, Russia) (CoKα radiation) (2θ angles: from 10 to 120°, step size: 0.1°, exposure time per step: 5 s, beam size: 6–8 mm).

2.5. Optical Microscopy

Optic histological study of the implantations zones was carried out using "Leica DM2500 DFC" light microscope (Leica Microsystems GmbH, Wetzlar, Germany).

2.6. Mechanical Testing

The tensile mechanical tests of the composites were carried out on a Zwick Z 020 universal testing machine (Zwick Roell Group, Ulm, Germany) at a displacement rate of 10 mm/min at room temperature. For the tensile tests, samples with 80 mm length, 5 mm width, and 2 mm thickness were

used. For the tests, 10–12 samples were investigated for the metallic glass ribbon and three samples for the tensile tests of each composite and pure PCL. The composite and pure PCL samples for the tensile tests were prepared in an APVM-904 thermal pressing machine (OJSC "NITI-Tesar", Saratov, Russia) at 120 °C. The metallic glass ribbon was used directly in the universal testing machine.

The density of the acquired materials was measured via a hydrostatic weighing method using an AND GR-202 analytical balance (A&D COMPANY Ltd., Tokyo, Japan) and an AND AD-1653 set (A&D COMPANY Ltd., Tokyo, Japan) for density determination in ethanol.

2.7. Laser Flash Analysis

Thermal diffusivity analysis of the obtained samples was done with a Netsch LFA 447 device (Netzsch Erich Netzsch GmbH & Co., Selb, Upper Franconia, Bavaria, Germany) (under argon flow). The temperature range for the investigation of the samples was set between 25 and 60 °C. The composite and PCL circular disk samples for the thermal analysis were prepared in an APVM-904 thermal pressing machine at 120 °C each. For the metallic glass ribbon, the circular disk sample was too brittle and thin; hence, thermal analysis of the sample was not possible.

2.8. DSC Analysis

The thermal stability and heat capacity of the samples were measured via differential scanning calorimetry (DSC) using a NETZSCH F1 Phoenix calorimeter (Netzsch Erich Netzsch GmbH & Co., Selb, Upper Franconia, Bavaria, Germany) under purified argon with 99.99% purity. The heating rate was ~10 °C/min under a flow of purified argon. The determination of the heat capacity of the composites was realized by comparison with a sapphire standard. The mass of the samples was 10–15 mg. The thermal conductivity was examined according to the ASTM E1461 standard, as outlined in our previous work [38,41,42].

2.9. In Vivo Studies

For the in vivo studies, round samples (metallic ribbon, PCL and 75/25) with a diameter of 8 mm and 1 mm thickness were used. Male C57/BL laboratory mice of 20–25 g weight were used. The animals were placed in big ventilated cages with food and water ad libitum. The animal study was approved by the ethical committee of the Research Institute of Human Morphology. All manipulations with animals were made according to the ethical guidelines. The skin of the mice was disinfected with 70% ethanol before implantation. Surgery was performed under isofluorane anesthesia. Samples were implanted subcutaneously into the back region of the mice. To check the reaction of the organism to the implantation and check possible resorption, pure PCL and 25/75 composite samples were implanted for 20 and 90 days. Glass samples were implanted for 10 and 90 days because the glass had higher bioactivity. Each group contained five animals, and one sample was implanted into one animal. After the animals were sacrificed, the samples with surrounding tissues were taken out for histological study. The presence of the sample in the implantation zone, the condition of the sample, and the presence/absence of the inflammation were studied.

3. Results

The composite samples were prepared with PCL/MGs weight ratios of 50/50, 75/25, and 90/10. To evaluate the polymer/metal composition with the best mechanical properties, the tensile properties of the different samples were measured after extrusion. The 75/25 (PCL/ MGs) composite samples exhibited the best properties among the investigated composites. The maximum tensile strength of these samples (Figure 1c) was 18.9 ± 1.7 MPa; the ultimate elongation was 462 ± 25% and Young's modulus 822 ± 35 MPa. The 50/50 composite samples had the highest Young's modulus (1799 ± 59 MPa) among the investigated composite samples. This was because of the higher content of the metallic glass. The other samples had less favorable properties with respect to their tensile plasticity and

strength (Table 1). Therefore, all subsequent tests and bio-experiments were carried out using the 75/25 composite samples.
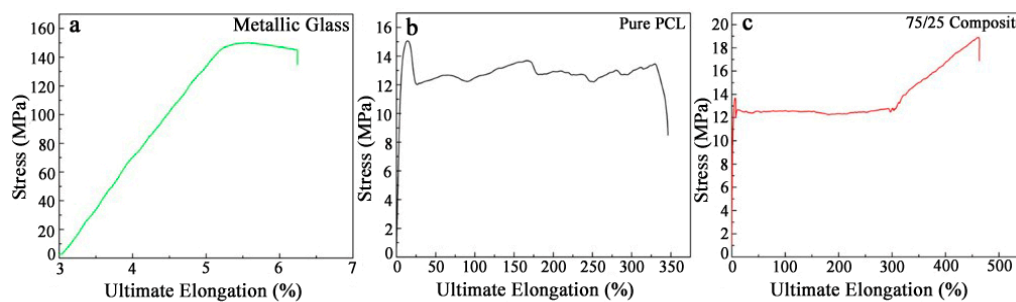

Figure 1. Tensile engineering stress-strain curves for (**a**) $Mg_{66}Zn_{30}Ca_4$ glassy ribbon, (**b**) pure polycaprolactone, and (**c**) $Mg_{66}Zn_{30}Ca_4$/PCL 75/25 composite.

Table 1. Mechanical properties of the obtained samples.

Samples	Young Modulus (MPa)	Tensile Strength (MPa)	Elongation (%)
PCL	351 ± 20	15.2 ± 3	352 ± 70
50/50 composite	1799 ± 60	12.7 ± 4.4	240 ± 60
75/25 composite	822 ± 35	18.9 ± 1.7	462 ± 25
90/10 composite	486 ± 45	18.6 ± 2.8	500 ± 55
Metallic Glass	31639 ± 75	150.2 ± 18.5	4 ± 0.2

The thermal behavior of all three types of samples (75/25 composite, PCL, and Mg-based MG) was studied via differential scanning calorimetry (DSC), as shown in Figure 2a. The sharp endothermic peak at 60 ± 0.1 °C indicates the melting temperature of pure PCL. The DSC curve of the metallic glass reveals a glass transition temperature T_g of 119 ± 0.1 °C and an onset temperature of crystallization T_x of 139 ± 0.1 °C, resulting in a supercooled liquid region $\Delta T_x = T_x - T_g$ of 20 ± 0.1 °C.
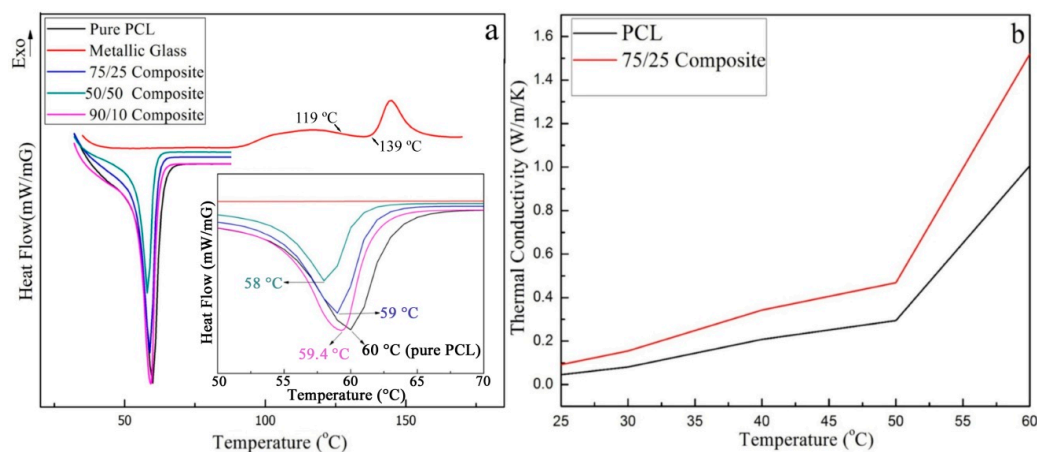

Figure 2. DSC thermographs for (**a**) $Mg_{66}Zn_{30}Ca_4$ metallic glass, pure PCL, and different metallic glass/PCL composites; (**b**) thermal conductivity of the pure PCL and 75/25 composite samples. The melting points of the pure PCL and composites samples under higher magnification in the insert.

Thermal resistivity analysis was carried out from 25 to 60 °C (Figure 2b). Table 2 shows that the thermal conductivity of the given samples increases with temperature, because of the brittle nature and thin samples; it was not possible to produce samples for thermal conductivity measurement from the pure metallic glass ribbon.

Table 2. Thermal properties and densities of the obtained samples.

Temperature Analysis, °C	25	30	40	50	60
PCL					
Thermal diffusivity, mm²/s	0.103 ± 0.03	0.1 ± 0.03	0.098 ± 0.04	0.097 ± 0.02	0.096 ± 0.03
Thermal conductivity, W/(m·K)	0.05 ± 0.01	0.08 ± 0.01	0.21 ± 0.01	0.29 ± 0.01	1.01 ± 0.02
Heat capacity, J/(g·K)	0.4 ± 0.02	0.74 ± 0.03	1.92 ± 0.14	2.75 ± 0.17	9.53 ± 0.2
Sample density, g/cm³			1.1 ± 0.02		
Composite (75/25)					
Thermal diffusivity, mm²/s	0.171 ± 0.04	0.165 ± 0.04	0.155 ± 0.03	0.1457 ± 0.04	0.135 ± 0.03
Thermal conductivity, W/(m·K)	0.09 ± 0.005	0.15 ± 0.007	0.35 ± 0.01	0.47 ± 0.012	1.52 ± 0025
Heat capacity, J/(g·K)	0.4 ± 0.03	0.7 ± 0.05	1.64 ± 0.12	2.4 ± 0.16	8.4 ± 0.22
Sample density, g/cm³			1.34 ± 0.02		
Composite (50/50)					
Thermal diffusivity, mm²/s	0.187 ± 0.03	0.183 ± 0.03	0.171 ± 0.04	0.16 ± 0.05	0.145 ± 0.05
Thermal conductivity, W/(m·K)	0.16 ± 0.02	0.3 ± 0.04	0.42 ± 0.05	0.55 ± 0.09	1.57 ± 0.11
Heat capacity, J/(g·K)	0.5 ± 0.05	0.95 ± 0.07	1.45 ± 0.13	2.02 ± 0.21	6.44 ± 0.26
Sample density, g/cm³			1.68 ± 0.02		

The XRD pattern of the $Mg_{66}Zn_{30}Ca_4$ ribbon obtained by melt spinning shows that the material was amorphous. A broad scattering signal was found at $2\theta = 38°$ for the metallic glass ribbon (Figure 3a). The XRD investigation of the pure PCL samples revealed a semicrystalline structure with two sharp peaks at $2\theta = 21.5°$ and $23.5°$ (Figure 3b). This finding is consistent with earlier works [30,31] and normal for this polymer. The semicrystallinity in the 75/25 composite stems from the PCL content (Figure 3c), i.e., the semicrystalline structure in the XRD pattern results from the polymer structure. However, it should be also noted that the production procedure proceeding in the supercooled liquid zone may induce nano-crystallization of the metallic glass sample, but is hard to detect [44].
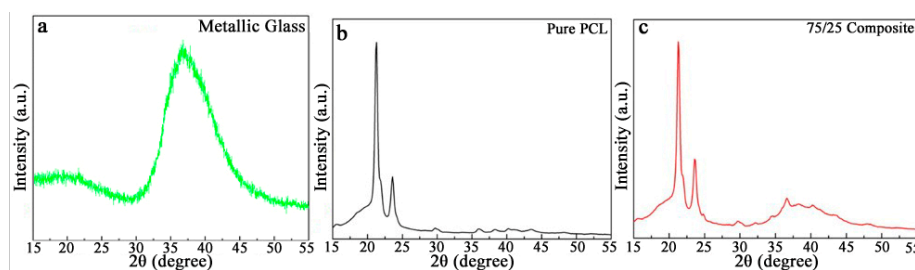

Figure 3. X-ray difraction patterns of the (**a**) metallic glass, (**b**) PCL, and (**c**) $Mg_{66}Zn_{30}Ca_4$/PCL 75/25 composite.

In vitro analysis for the Mg-Zn-Ca metallic glass has been previously performed [29], revealing that this metallic glass is non-toxic and biocompatible. PCL has already been proven to be biocompatible [45]. In the present study, in vivo studies have been carried out using three types of materials: pure MG, pure PCL, and the 75/25 composite with the relatively optimal mechanical properties. Samples of pure PCL and 75/25 composite were covered with connective tissue. The size and shape of the samples remained unchanged. There were no signs of bio-destruction, and the line of connective tissue was smooth (Figure 4a–d). The samples remained in the implantation zone and did not cause tissue destruction in the adjacent tissues in all five animals of both groups. The pure metallic glass caused inflammation, that is, an abscess was found in the implantation zone in all five animals (Figure 4e,f). The size of the abscess decreased with time over 90 days, and bio-destruction of the sample occurred.

No gas pockets were observed in the animals with the implanted metallic glass ribbon after 90 days (Figure 4f).
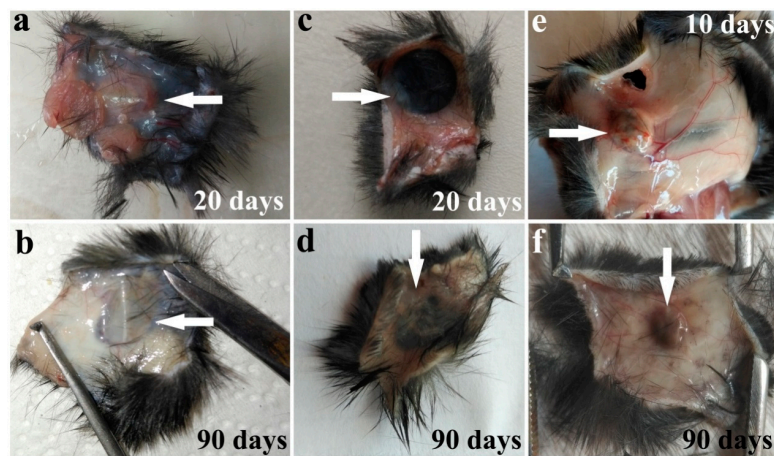

Figure 4. Photos of the implantation zones (marked by arrows) of a PCL (**a**,**b**) 75/25 composite (**c**,**d**) and metallic glass sample (**e**,**f**). PCL sample (**a**,**b**) and 75/25 composite sample (**c**,**d**) stayed in the implantation zone, maintained its shape and size, and did not cause inflammation; pure glass sample (**e**,**f**) caused the abscess in the implantation zone and was resorbed.

Microscopic studies of the PCL and 75/25 composite samples showed a smooth line of connective tissue on the tissue-material border, the absence of inflammation, and a few cells from foreign bodies and blood vessels in the connective tissue (Figure 5a–d). The metallic glass caused inflammation, and cellular infiltration macrophages and neutrophils were noticed in the implantation zone (Figure 5e,f).
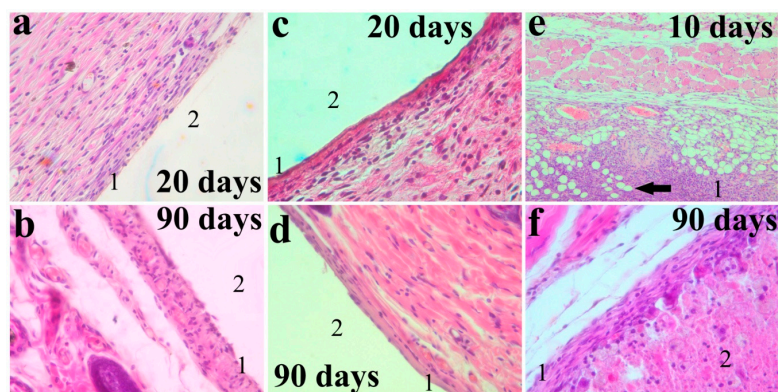

Figure 5. Micrographs of the implantation zone of the PCL (**a**,**b**), 75/25 composite (**c**,**d**), and metallic glass sample (**e**,**f**). (**a**) The smooth line of connective tissue (1) between the implantation zone (2) and tissues of the organism; no signs of inflammation and destruction of the tissues; hematoxylin and eosin staining; and magnification of 400×. (**b**) The smooth line of connective tissue (1) between the zone of implantation (2) and tissues of the organism; no signs of inflammation and destruction of the tissues; hematoxylin and eosin staining; and magnification of 400×. (**c**) The smooth line of connective tissue (1) between the implantation zone (2) and tissues of the organism; no signs of inflammation and destruction of the tissues; hematoxylin and eosin staining; and magnification of 400×. (**d**) The smooth line of connective tissue (1) between the implantation zone (2) and tissues of the organism; no signs of inflammation and destruction of the tissues; hematoxylin and eosin staining; and magnification of 400×. (**e**) Inflammation, neutrophil, and macrophages cell infiltration in the implantation zone and gas bubbles (marked by an arrow); the sample underwent bio-destruction; hematoxylin and eosin staining; and magnification of 100×. (**f**) Inflammation, connective tissue (1) surrounds the implantation zone filled with macrophages and cell detritus (2); the sample underwent bio-destruction; hematoxylin and eosin staining; and magnification of 400×.

After analyzing the acquired results, it was possible to conclude that the 75/25 composite was promising for further in vivo studies. The glass samples caused inflammation, which made them unsuitable for further studies (Table 3).

Table 3. Resultsof the in vivo study.

Experimental Group	Resorption	Inflammation	Gas Production	Summary
PCL 20 days	-	-	-	Perspective sample, for further studies
PCL 90 days	-	-	-	
Composite 20 days	-	-	-	Perspective sample, for further studies
Composite 90 days	-	-	-	
Mg-Glass 10 days	Resorbed	Large abscess	Microscopic gas bubbles in the zone of implantation	Cannot be used as a biomaterial for an implant because of excessive inflammation
Mg-Glass 90 days	Resorbed	Small abscess	-	

4. Discussion

Generally, metallic glasses are brittle in nature, but the present Mg-based metallic glass displayed some plastic deformation (Figure 1a) in addition to the expected elastic deformation [46]. This plastic behavior is linked to shear band formation and propagation occurring during the tensile test. Metallic glasses are prone to shear band formation at room temperature [47]. Shear bands are important in metallic glasses because they play a major role in the plasticity and failure at room temperature. The ductility of the Mg-based metallic glass was poor, and the shear bands occurred near the failure of the ribbon. The shear bands occurring along the plane close to the maximum shear stress and flow stress are due to local heating and disordering [48]. The short-range bond order usually increases with the heat of mixing of the constituent elements. This increase can cause a change in the atomic bond structure that affects local chemical inhomogeneity, which leads to the formation and propagation of shear bands [49,50]. For the case of pure PCL, lower tensile stress response was observed (15.2 ± 3 MPa), while the plastic deformation was found to be quite high because of its flexible nature (ultimate elongation of 352 ± 70%) (Figure 1b). The composite samples with a high percentage of PCL (75/25) showed a good ductility of more than 400%. In this regard, in the tensile tests, the (75/25) composite showed the best mechanical properties among the selected composites (Table 1).

The XRD pattern of the $Mg_{66}Zn_{30}Ca_4$ ribbon after the melt spinning process shows a broad diffraction maximum of around $2\theta = 38°$ (Figure 3a). The broad maximum indicates that the material was amorphous. XRD investigation of the pure PCL reveals two characteristic peaks (Figure 3b). The main peak is at $2\theta = 21.5°$, and a weak peak is visible at $2\theta = 23.5°$, which indicates the semicrystalline nature of the PCL. Because of the rather high PCL content, the 75/25 composite exhibits two characteristics peaks similar to pure PCL at $2\theta = 21.5°$ and $2\theta = 23.5°$. In addition, there is a broad amorphous maximum steaming from the metallic glass at $2\theta = 38°$ (Figure 3c).

The DSC curves of the $Mg_{66}Zn_{30}Ca_4$ ribbon, PCL, and different composites (75/25, 50/50, 90/10) were recorded using a heating rate of 10 °C/min. The results show that the metallic glass has a T_g of 119 ± 0.1 °C and a T_x of 139 ± 0.1 °C. The composite material was produced in the temperature range between 120 and 130 °C, which is in the supercooled region of the metallic glass and above the melting temperature of the polymer. As a result, the thermal properties of the composite samples prepared using the above-mentioned conditions were improved and had a good correlation with the data from our previous work [38,41,42]. For the 75/25 composite, the endothermic peak at 59 ± 0.1 °C reflects the melting of the PCL. Similarly, it was 58 ± 0.1 °C for the 50/50 composite and 59.4 ± 0.1 °C for the 90/10 composite. This finding suggests that the incorporation of reinforcement material (metallic glass) in the PCL matrix affects the thermal properties of the resulting composite. The slight decrease in the melting of the composites (see inset in Figure 2a) is due to the higher thermal conductivity of the metallic glass. Heat is transferred to the metallic glass, and due to this, the polymer starts to melt faster.

As a result, the melting peaks of the composite shift towards lower temperatures. These results were in good agreement with the work of Senatov et al. [51], which showed that the melting temperature of the polymer (position of the melting peak on the DSC curve) influences the dispersed filler addition. In this work, we have also associated this process with increasing in the polymer crystallinity. In this regard, the increasing of the PCL crystallinity should also be possible in the present research work. It should be also noted that the DSC curves (Figure 2a) suggest that the polymer and obtained composites are not stable at room temperature (because of the too narrow range of the experiment).

Accurate data are needed to understand the heat transfer mechanism in the tissue [52]; in this regard, the estimation of the thermal conductivity is very important. Thermal properties [53] are crucial in a biomaterial because they are needed to develop thermal models. Thermal models have the utmost significance in hyperthermia and therapeutic procedures. These procedures depend on heat delivery mechanisms like ultrasound, microwave, and radiofrequency. Heat transfer also plays a significant role in perfusion.

The thermal conductivity of the samples was calculated using [54]:

$$\lambda = \alpha \cdot C_p \cdot \rho \tag{1}$$

where α is the thermal diffusivity [mm^2/s], C_p is the specific heat capacity [J/g·K], and ρ is the sample density [g/cm^3].

The thermal conductivity and thermal diffusivity of the composite sample (50/50) are the highest compared with the PCL and MG 75/25 composite samples. This is because more metallic glass particles are present in the 50/50 composite sample, which shows that the thermal conductivity increases with an increasing amount of the Mg-based metallic glass.

The discontinuity in the thermal conductivity of the PCL and composite (Figure 2b) could be because during PCL melting, the heat capacity of the polymer changes significantly in this regard, and, according to equation (1), thermal conductivity changes too.

The 75/25 composite and pure PCL samples were suitable for further in vivo studies. No gas was released in the case of the (75/25) and PCL samples; however, the inflammation that occurred for the Mg-ribbon and gas bubbles was observed in the implantation zone; hence, it was not further considered for use as an implant. The results show that the composite samples can be recommended for further investigation, such as for orthotopical implantation into a bone defect.

The in vivo study showed that the tested PCL and composite materials are biocompatible. They remained at the implantation location covered with connective tissue, and there were no negative reactions in the implantation zone, such as acute inflammation or destruction of the surrounding tissues. These results allow us to conclude that PCL and the composite materials have significant potential for use as bone implants and are of interest for further studies because the normal reaction on implantation did not hinder the healing process [55]. However, the pure metallic glass is not biocompatible, and it caused substantial inflammation in the implantation zone, which is undesirable because it prevents healing, causes destruction, and hinders the integration of the material into the tissue. Additionally, multiple gas bubbles (presumed to be hydrogen) were observed in the zone of implantation, excessive amounts of which are harmful to the organism [56]. Small amounts of gas production may have a positive effect by creating mechanical stress [22] that stimulates bone formation, but excessive inflammation has to be avoided for such materials, thus rendering the glass unsuitable for further studies [23]. However, no gas production was observed after the implantation of the PCL/glass composite. After 90 days, the implantation zone still showed inflammation with cellular infiltration. Hence, it can be concluded that pure glass is not a promising material for bone implants.

5. Conclusions

The present study explored the applicability of metallic glass/PCL composites for repairing hard tissue defects. Mechanical alloying, combined with coextrusion, allowed for the successful preparation

of metallic glass/PCL composites. Physicochemical characterization confirmed the good blending of the metallic glass as reinforcement in the PCL matrix. The thermal conductivity of the composites increases with the addition of the Mg-based metallic glass. The mechanical properties suggest that the composites could be used for non-load-bearing applications. Pure $Mg_{66}Zn_{30}Ca_4$ glass causes excessive inflammation with hydrogen gas production, and thus the MG is not suitable as an implant material. Combining the glass with polymer solves this issue. Pure PCL and 75/25 PCL/MG composite samples are biologically inert, do not cause inflammation, and stay in the implantation location after 90 days. The current report confirms that metallic glass/PCL composites are promising for further investigation as a perspective material for biomedical applications.

Author Contributions: A.S. (Adit Sharma), A.K. analyzed the data, wrote, reviewed, and edited the manuscript; A.S. (Adit Sharma), M.Z., A.S. (Andrei Stepashkin), A.K., V.K., S.K. (Sergey Ketov), M.C., and V.Z. performed the experiments; J.-Q.W., D.L.-L., J.E., S.K. (Sergey Ketov), B.S., and H.K. contributed materials and analysis tools; V.Z., D.V., and S.K. (Sergey Kaloshkin) conceived and designed the experiments. All authors have read and agreed to the published version of the manuscript.

Conflicts of Interest: The authors declare no conflict of interest.

Ethic Approval: All experiments with animals were performed in compliance with ethical requirements, approved by the Ethical commission of Research Institute of Human Morphology (№21a from 15 January 2019).

References

1. Granel, H.; Bossard, C.; Nucke, L.; Wauquier, F.; Rochefort, G.Y.; Guicheux, J.; Jallot, E.; Lao, J.; Wittrant, Y. Optimized Bioactive Glass: The Quest for the Bony Graft. *Adv. Healthc. Mater.* **2019**, *8*, e1801542. [CrossRef] [PubMed]

2. Amini, A.R.; Laurencin, C.T.; Nukavarapu, S.P. Bone tissue engineering: Recent advances and challenges. *Crit. Rev. Biomed. Eng.* **2012**, *40*, 363–408. [CrossRef]

3. Ebraheim, N.A.; Elgafy, H.; Xu, R. Bone-Graft Harvesting From Iliac and Fibular Donor Sites: Techniques and Complications. *J. Am. Acad. Orthop. Surg.* **2001**, *9*, 210–218. [CrossRef] [PubMed]

4. Urabe, K.; Itoman, M.; Toyama, Y.; Yanase, Y.; Iwamoto, Y.; Ohgushi, H.; Ochi, M.; Takakura, Y.; Hachiya, Y.; Matsuzaki, H.; et al. Current trends in bone grafting and the issue of banked bone allografts based on the fourth nationwide survey of bone grafting status from 2000 to 2004. *J. Orthop. Sci.* **2007**, *12*, 520–525. [CrossRef]

5. Kim, Y.; Rodríguez, A.E.; Nowzari, H. The Risk of Prion Infection through Bovine Grafting Materials. *Clin. Implant. Dent. Relat. Res.* **2016**, *18*, 1095–1102. [CrossRef] [PubMed]

6. Freed, L.E.; Grande, D.A.; Lingbin, Z.; Emmanual, J.; Marquis, J.C.; Langer, R. Joint resurfacing using allograft chondrocytes and synthetic biodegradable polymer scaffolds. *J. Biomed. Mater. Res.* **1994**, *28*, 891–899. [CrossRef] [PubMed]

7. Williams, D.F. On the mechanisms of biocompatibility. *Biomaterials* **2008**, *29*, 2941–2953. [CrossRef] [PubMed]

8. Song, G. Control of biodegradation of biocompatable magnesium alloys. *Corros. Sci.* **2007**, *49*, 1696–1701. [CrossRef]

9. Ilich, J.Z.; Kerstetter, J.E. Nutrition in bone health revisited: A story beyond calcium. *J. Am. Coll. Nutr.* **2001**, *19*, 715–737. [CrossRef]

10. Le, Q.; Zhang, Z.; Shao, Z.-W.; Cui, J.; Xie, Y. Microstructures and mechanical properties of Mg-2%Zn-0.4%RE alloys. *Trans. Nonferrous Met. Soc. China* **2010**, *20*, s352–s356. [CrossRef]

11. Dezfuli, S.N.; Huan, Z.; Mol, A.; Leeflang, S.; Chang, J.; Zhou, J. Advanced bredigite-containing magnesium-matrix composites for biodegradable bone implant applications. *Mater. Sci. Eng. C* **2017**, *79*, 647–660. [CrossRef] [PubMed]

12. Lieberman, J.R.; Friedlaender, G.E. *Bone Regeneration and Repair: Biology and Clinical Applications*; Humana Press: Totowa, NJ, USA, 2005; ISBN 0896038475.

13. Faryadi, Q. The Magnificent Effect of Magnesium to Human Health: A Critical Review. *Int. J. Appl. Sci. Technol.* **2012**, *2*, 118–126.

14. Bommala, V.K.; Krishna, M.G.; Rao, C.T. Magnesium matrix composites for biomedical applications: A review. *J. Magnes. Alloy.* **2019**, *7*, 72–79. [CrossRef]

15. Ali, W.; Mehboob, A.; Han, M.-G.; Chang, S.-H. Experimental study on degradation of mechanical properties of biodegradable magnesium alloy (AZ31) wires/poly(lactic acid) composite for bone fracture healing applications. *Compos. Struct.* **2019**, *210*, 914–921. [CrossRef]

16. Haghshenas, M. Mechanical characteristics of biodegradable magnesium matrix composites: A review. *J. Magnes. Alloy.* **2017**, *5*, 189–201. [CrossRef]

17. Rupert, T.J.; Trenkle, J.C.; Schuh, C.A. Enhanced solid solution effects on the strength of nanocrystalline alloys. *Acta Mater.* **2011**, *59*, 1619–1631. [CrossRef]

18. Wong, P.-C.; Tsai, P.-H.; Li, T.-H.; Cheng, C.; Jang, J.; Huang, J. Degradation behavior and mechanical strength of Mg-Zn-Ca bulk metallic glass composites with Ti particles as biodegradable materials. *J. Alloy. Compd.* **2017**, *699*, 914–920. [CrossRef]

19. Yang, J.; Cui, F.Z.; Lee, I.S.; Wang, X. Plasma surface modification of magnesium alloy for biomedical application. *Surf. Coatings Technol.* **2010**, *205*, S182–S187. [CrossRef]

20. Chen, J.; Tan, L.; Yu, X.; Etim, I.P.; Ibrahim, M.; Yang, K. Mechanical properties of magnesium alloys for medical application: A review. *J. Mech. Behav. Biomed. Mater.* **2018**, *87*, 68–79. [CrossRef]

21. Swain, S.K.; Gotman, I.; Unger, R.E.; Kirkpatrick, C.J.; Gutmanas, E.Y. Microstructure, mechanical characteristics and cell compatibility of β-tricalcium phosphate reinforced with biodegradable Fe-Mg metal phase. *J. Mech. Behav. Biomed. Mater.* **2016**, *53*, 434–444. [CrossRef] [PubMed]

22. Zberg, B.; Uggowitzer, P.J.; Löffler, J.F. MgZnCa glasses without clinically observable hydrogen evolution for biodegradable implants. *Nat. Mater.* **2009**, *8*, 887–891. [CrossRef] [PubMed]

23. Zimmermann, T.; Ferrandez-Montero, A.; Lieblich, M.; Ferrari, B.; González-Carrasco, J.L.; Müller, W.-D.; Schwitalla, A. In vitro degradation of a biodegradable polylactic acid/magnesium composite as potential bone augmentation material in the presence of titanium and PEEK dental implants. *Dent. Mater.* **2018**, *34*, 1492–1500. [CrossRef] [PubMed]

24. Yamamoto, A.; Hiromoto, S. Effect of inorganic salts, amino acids and proteins on the degradation of pure magnesium in vitro. *Mater. Sci. Eng. C* **2009**, *29*, 1559–1568. [CrossRef]

25. Zhang, E.; Xu, L.; Yu, G.; Pan, F.; Yang, K. In vivo evaluation of biodegradable magnesium alloy bone implant in the first 6 months implantation. *J. Biomed. Mater. Res. Part A* **2009**, *90*, 882–893. [CrossRef] [PubMed]

26. Louzguine-Luzgin, D. *Bulk Metallic Glasses and Glassy/Crystalline Materials*; Springer: Berlin/Heidelberg, Germany, 2016; Volume 231, pp. 397–440.

27. Zheng, Y.; Xu, X.; Xu, Z.; Wang, J.Q.; Cai, H. *Metallic Biomaterials: New Directions and Technologies*; John Wiley & Sons: Weinheim, Germany, 2017; ISBN 9783527341269.

28. Gu, X.; Zheng, Y.; Zhong, S.; Xi, T.; Wang, J.; Wang, W. Corrosion of, and cellular responses to Mg–Zn–Ca bulk metallic glasses. *Biomaterials* **2010**, *31*, 1093–1103. [CrossRef]

29. Yu, H.-J.; Wang, J.-Q.; Shi, X.; Louzguine-Luzgin, D.; Wu, H.-K.; Perepezko, J.H. Ductile Biodegradable Mg-Based Metallic Glasses with Excellent Biocompatibility. *Adv. Funct. Mater.* **2013**, *23*, 4793–4800. [CrossRef]

30. Nair, L.S.; Laurencin, C.T. Biodegradable polymers as biomaterials. *Prog. Polym. Sci.* **2007**, *32*, 762–798. [CrossRef]

31. Chan, D.S.; Fnais, N.; Ibrahim, I.; Daniel, S.J.; Manoukian, J. Exploring polycaprolactone in tracheal surgery: A scoping review of in-vivo studies. *Int. J. Pediatr. Otorhinolaryngol.* **2019**, *123*, 38–42. [CrossRef]

32. Guerra, A.J.; Ciurana, J. 3D-printed bioabsordable polycaprolactone stent: The effect of process parameters on its physical features. *Mater. Des.* **2018**, *137*, 430–437. [CrossRef]

33. Dwivedi, R.; Kumar, S.; Pandey, R.; Mahajan, A.; Nandana, D.; Katti, D.S.; Mehrotra, D. Polycaprolactone as biomaterial for bone scaffolds: Review of literature. *J. Oral Biol. Craniofacial Res.* **2020**, *10*, 381–388. [CrossRef] [PubMed]

34. Koenig, M.; Huang, S. Biodegradable blends and composites of polycaprolactone and starch derivatives. *Polymer* **1995**, *36*, 1877–1882. [CrossRef]

35. Kim, I.A.; Rhee, S.-H. Preparation of a Non-Woven Poly(ε-caprolactone) Fabric with Partially-Embedded Apatite Surface for Bone Tissue Engineering Applications by Partial Surface Melting of Poly(ε-caprolactone) Fibers. *J. Biomed. Mater. Res. Part A* **2017**, *105*, 1973–1983. [CrossRef] [PubMed]

36. Nie, W.; Gao, Y.; McCoul, D.J.; Gillispie, G.J.; Zhang, Y.; Liang, L.; He, C. Rapid mineralization of hierarchical poly(l-lactic acid)/poly(ε-caprolactone) nanofibrous scaffolds by electrodeposition for bone regeneration. *Int. J. Nanomed.* **2019**, *14*, 3929–3941. [CrossRef]

37. Kündig, A.; Schweizer, T.; Schafler, E.; Löffler, J.F. Metallic glass/polymer composites by co-processing at similar viscosities. *Scr. Mater.* **2007**, *56*, 289–292. [CrossRef]

38. Zadorozhnyy, V.Y.; Chukov, D.; Churyukanova, M.; Gorshenkov, M.; Stepashkin, A.; Tsarkov, A.; Louzguine-Luzgin, D.; Kaloshkin, S. Investigation of contact surfaces between polymer matrix and metallic glasses in composite materials based on high-density polyethylene. *Mater. Des.* **2016**, *92*, 306–312. [CrossRef]

39. Wang, Z.; Georgarakis, K.; Nakayama, K.S.; Li, Y.; Tsarkov, A.; Xie, G.; Dudina, D.V.; Louzguine-Luzgin, D.; Yavari, A.R. Microstructure and mechanical behavior of metallic glass fiber-reinforced Al alloy matrix composites. *Sci. Rep.* **2016**, *6*, 24384. [CrossRef]

40. Bowman, H.F.; Cravalho, E.G.; Woods, M. Theory, Measurement, and Application of Thermal Properties of Biomaterials. *Annu. Rev. Biophys. Bioeng.* **1975**, *4*, 43–80. [CrossRef]

41. Zadorozhnyy, V.Y.; Gorshenkov, M.; Churyukanova, M.; Stepashkin, A.; Moskovskikh, D.; Ketov, S.; Zinnurova, L.; Sharma, A.; Louzguine-Luzgin, D.; Kaloshkin, S. Investigation of structure and thermal properties in composite materials based on metallic glasses with small addition of polytetrafluoroethylene. *J. Alloy. Compd.* **2017**, *707*, 264–268. [CrossRef]

42. Zadorozhnyy, V.Y.; Churyukanova, M.; Stepashkin, A.; Zadorozhnyy, V.Y.; Sharma, A.; Moskovskikh, D.; Wang, J.-Q.; Shabanova, E.; Ketov, S.; Luzguine-Luzgin, D.V.; et al. Structure and Thermal Properties of an Al-Based Metallic Glass-Polymer Composite. *Metals* **2018**, *8*, 1037. [CrossRef]

43. Zadorozhnyy, V.Y.; Shelekhov, E.V.; Milovzorov, G.S.; Strugova, D.V.; Zinnurova, L.K. Analysis of the Background Temperature During the Mechanical Alloying of Metal Powders in the Planetary Ball Mill. *Inorg. Mater. Appl. Res.* **2018**, *9*, 559–565. [CrossRef]

44. Ketov, S.; Shi, X.; Xie, G.; Kumashiro, R.; Churyumov, A.Y.; Bazlov, A.I.; Chen, N.; Ishikawa, Y.; Asao, N.; Wu, H.; et al. Nanostructured Zr-Pd Metallic Glass Thin Film for Biochemical Applications. *Sci. Rep.* **2015**, *5*, 7799. [CrossRef]

45. Serrano, M.C.; Pagani, R.; Vallet-Regı, M.; Peña, J.; Rámila, A.; Izquierdo, I.; Portolés, M.T. In vitro biocompatibility assessment of poly(ε-caprolactone) films using L929 mouse fibroblasts. *Biomaterials* **2004**, *25*, 5603–5611. [CrossRef] [PubMed]

46. Greer, A.; Cheng, Y.; Ma, E. Shear bands in metallic glasses. *Mater. Sci. Eng. R Rep.* **2013**, *74*, 71–132. [CrossRef]

47. Torki, M.E.; Benzerga, A.A. A mechanism of failure in shear bands. *Extrem. Mech. Lett.* **2018**, *23*, 67–71. [CrossRef]

48. Louzguine-Luzgin, D.; Jiang, J.; Bazlov, A.; Zolotorevzky, V.; Mao, H.; Ivanov, Y.P.; Greer, A. Phase separation process preventing thermal embrittlement of a Zr-Cu-Fe-Al bulk metallic glass. *Scr. Mater.* **2019**, *167*, 31–36. [CrossRef]

49. Park, E.-S.; Kyeong, J.; Kim, D. Enhanced glass forming ability and plasticity in Mg-based bulk metallic glasses. *Mater. Sci. Eng. A* **2007**, *449*, 225–229. [CrossRef]

50. Park, E.-S.; Kim, D.; Ohkubo, T.; Hono, K. Enhancement of glass forming ability and plasticity by addition of Nb in Cu-Ti-Zr-Ni-Si bulk metallic glasses. *J. Non-Cryst. Solids* **2005**, *351*, 1232–1238. [CrossRef]

51. Senatov, F.; Niaza, K.; Zadorozhnyy, V.Y.; Maksimkin, A.; Kaloshkin, S.; Estrin, Y. Mechanical properties and shape memory effect of 3D-printed PLA-based porous scaffolds. *J. Mech. Behav. Biomed. Mater.* **2016**, *57*, 139–148. [CrossRef] [PubMed]

52. Valvano, J.W.; Cochran, J.R.; Diller, K.R. Thermal conductivity and diffusivity of biomaterials measured with self-heated thermistors. *Int. J. Thermophys.* **1985**, *6*, 301–311. [CrossRef]

53. Bhavaraju, N.; Cao, H.; Yuan, D.; Valvano, J.; Webster, J.G. Measurement of directional thermal properties of biomaterials. *IEEE Trans. Biomed. Eng.* **2001**, *48*, 261–267. [CrossRef]

54. Maksimkin, A.; Senatov, F.; Anisimova, N.; Kiselevskii, M.V.; Zalepugin, D.; Chernyshova, I.; Tilkunova, N.; Kaloshkin, S. Multilayer porous UHMWPE scaffolds for bone defects replacement. *Mater. Sci. Eng. C* **2017**, *73*, 366–372. [CrossRef] [PubMed]

55. Khorramirouz, R.; Go, J.; Noble, C.; Jana, S.; Maxson, E.; Lerman, A.; Young, M. A novel surgical technique for a rat subcutaneous implantation of a tissue engineered scaffold. *Acta Histochem.* **2018**, *120*, 282–291. [CrossRef] [PubMed]

56. Noviana, D.; Paramitha, D.; Ulum, M.F.; Hermawan, H. The effect of hydrogen gas evolution of magnesium implant on the postimplantation mortality of rats. *J. Orthop. Transl.* **2015**, *5*, 9–15. [CrossRef] [PubMed]